FLOW REGIMES OF MISCIBLE FLUIDS IN A HELE-SHAW CELL

VICTORIA-ELENA PLOPEANU*, CLAUDIU PATRASCU

Hydraulics Department, POLITEHNICA Bucharest,
Splaiul Independentei 313, 060042, Bucharest, Romania
Corresponding author*: victoria.plopeanu@stud.fim.upb.ro

Received March 20, 2025

Abstract. The present study investigates the flow dynamics of viscous fluid threads interacting with a less viscous fluid and their stability as they flow through a Hele-Shaw microfluidic cell. We study multiple liquid pairs and identify for the first time several flow regimes, including the well-known Kelvin-Helmholtz instability.

Key words: Hele-Shaw cell, fluid threads, hydrodynamic instability.

DOI: https://doi.org/10.59277/RomJPhys.2025.70.910

1. INTRODUCTION

Multi-fluid flows and interfaces have been extensively studied in microfluidic devices due to their capability of transporting and manipulating a variety of materials at the microscale.

Early studies have been conducted using relatively low viscosity fluids [1–4]. For fluids with high viscosity, as the dimensions of the channel decrease, the hydraulic resistance increases significantly, making it difficult to reduce the large pressure drop required to displace the fluids in the highly confined microchannel [5]. However, there are some specific applications where the working fluids have large viscosity contrasts. Such examples include the need to increase the viscosity of a fluid by adding a viscosifier or to decrease the viscosity of a thick material (such as a petroleum product) by incorporating a thinner [6]. As a result, various microfluidic methods and geometries have been implemented to enhance mixing of highly viscous fluids at small scales.

Previous investigations performed in Hele-Shaw configurations were conducted with miscible liquid pairs such as silicone oils as working fluids [7, 8]. These polymeric oils displayed a broad range of instabilities such as folding, threading and piling. Other experimental studies have established the role of the interfacial tension by adding surfactants to the immiscible fluid phases [9–11]. The study resulted in a method to generate droplets periodically and several observations on different flow patterns that were induced by the low interfacial tension.

The field of microfluidics has facilitated the study of fluid flows in the absence of significant gravitational effects. One notable advantage of microfluidic devices is

the reduced liquid volumes required to proceed the experiments, which can find use in point-of-care (POC) applications for early medical detection of infections [12–14].

Such microfluidic devices can be used in the field of chemical engineering as a method to produce complex soft materials, such as emulsions [15–17] and foams [18, 19], due to their capability to enhance mixing between miscible fluids and initiate emulsification processes between immiscible fluids. When considering immiscible liquid pairs, interfacial tension is the relevant parameter to control the encapsulation of complex materials [20].

The present paper investigates multi-fluid flows at the microscale in a Hele-Shaw cell. In the following sections we present several unstable flow regimes of miscible fluid pairs in such microfluidic chambers. We emphasize scaling laws that help us quantify the experimental observations.

2. EXPERIMENTAL DETAILS

2.1. THE MANUFACTURING PROCESS OF THE MICROCHANNEL

Microfluidic devices offer a new experimental framework for investigating multi-fluid flows at the microscale. In this study, we investigate the transport of fluids in microfluidic devices that were manufactured using photolithography on a silicon wafer. The characteristic dimensions of the microchannel are depicted in Fig. 1a.

The microgeometry consists of four consecutive elements, including: (1) a right angle hydrodynamic flow focusing section with square microchannels, (2) an inlet microchannel, (3) a Hele-Shaw cell and (4) an outlet square microchannel. The height of the device is 100 μm.

The term Hele-Shaw cell refers to the space generated by the gap between two plane parallel plates. The device is characterized by a large chamber aspect ratio $w/h = 20$. This configuration presents two main characteristics that are essential in the study of multiphase flows and the different hydrodynamic instabilities that may occur. On one hand, the transparent cell provides increased visibility of the flow. On the other hand, given the large aspect ratio, the flow inside the cell can be well described by a two-dimensional approximation, the Hele-Shaw approximation. This experimental approach holds the promise for practical use in fields such as the synthesis of colloidal particles, protein crystallization and biomaterials encapsulation [5, 9].

The microfluidic devices were manufactured using photolithography on a 4 inches silicon wafer. Photolithography is a fabrication process that utilizes UV radiation to expose the geometric designs onto a light-sensitive photoresist layer. The purpose is to transfer them to the underlying substrate. The photoresist is selectively exposed to the UV radiation through a mask that contains an opaque model. This results in

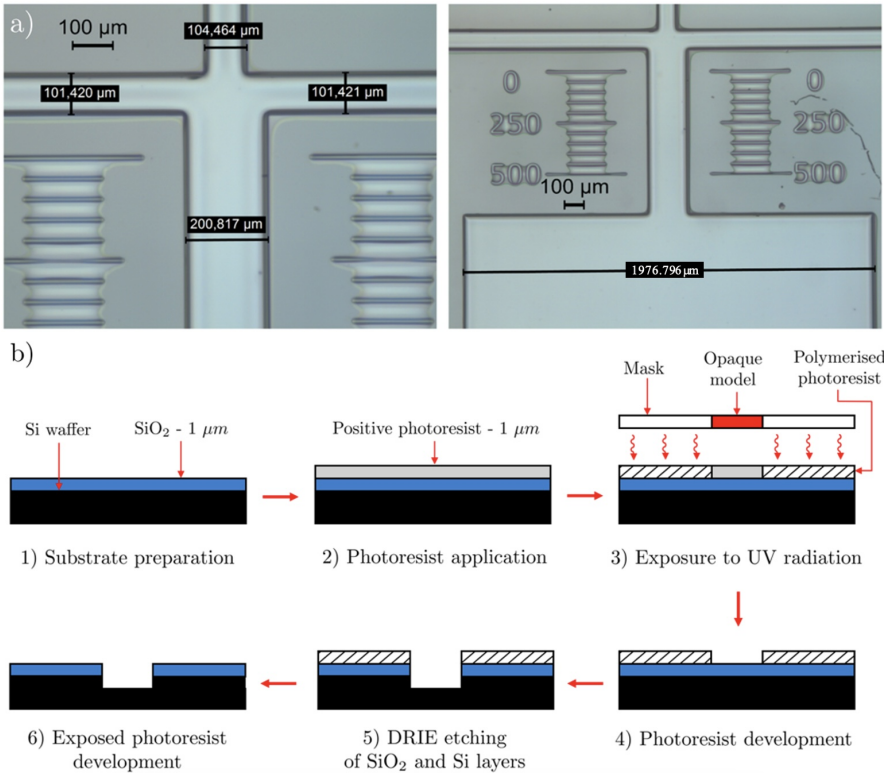

Fig. 1 – (a) Dimensions of the Hele-Shaw cell. (b) Schematic representation of the photolithographic process.

a pattern in the photoresist that can be developed and selectively dissolved to reveal the design of the microchannels on the underlying substrate. Figure 1b describes the photolithographic patterning process.

The polymer poured over the silicon mould is polydimethylsiloxane - PDMS. The polymerized PDMS is then peeled off the silicon wafer. A biomedical forceps with an outer diameter of 1 mm is used to make the holes corresponding to the microfluidic inlet and outlet ports. The resulted microchannel is chemically bonded to a glass slide that seals it. Microfluidic ports are created from copper tubes with an outer diameter of 1 mm and an approximate length of 1 cm. Microfluidic tubing is attached to the created ports.

2.2. EXPERIMENTAL SETUP

To experimentally study and visualize flow regimes in the Hele-Shaw cell, we use an inverted microscope equipped with a high-speed camera (Photron FASTCAM UX 100) recording at over 4000 frames per second. We inject miscible fluids in the microchannel through the microfluidic tubing with the aid of two syringe pumps. The miscible fluid pairs consist of two phases: water and solutions of water and glycerol having different viscosity contrasts (see Table 1).

Table 1

Fluid properties of the investigated liquid pairs

Dispersed phase	η_1 [mPa·s]	ρ_1 [kg/m^3]	Continuous phase	η_2 [mPa·s]	ρ_2 [kg/m^3]	χ
Water-glycerol sol.	20	1181	Water	1	998	20
Water-glycerol sol.	55	1209	Water	1	998	55
Water-glycerol sol.	100	1223	Water	1	998	100

The experimental setup is shown in Fig. 2. The dispersed phase represented by the more viscous fluid, having a viscosity η_1, is injected into the central channel at a volumetric flow rate Q_1. The less viscous fluid with a viscosity η_2, in this case the continuous phase, is symmetrically infused into the two side channels at a volumetric flow rate Q_2. We examine the flow dynamics over a range of flow rate ratios $\varphi = Q_1/Q_2$ and viscosity ratios $\chi = \eta_1/\eta_2$.

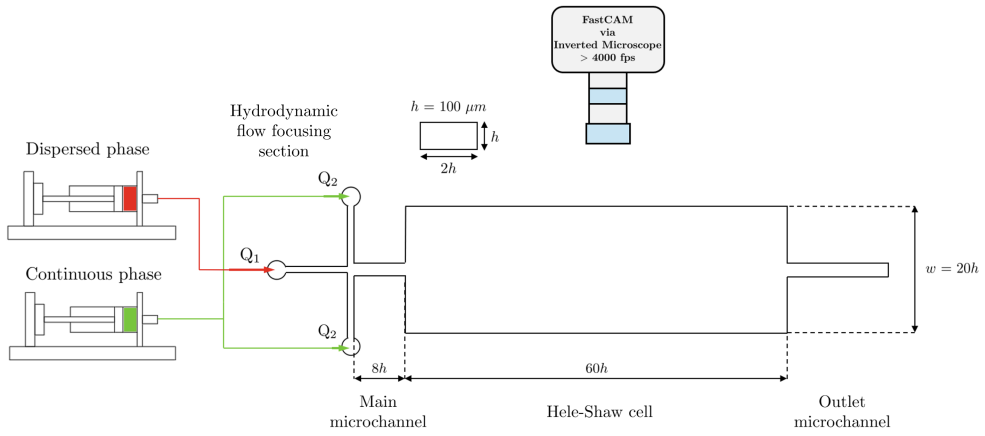

Fig. 2 – Schematic representation of the experimental setup.

3. RESULTS

3.1. A HYDRODYNAMIC INSTABILITY OF MISCIBLE FLUID THREADS

The flow configuration where the more viscous liquid is enveloped by the less viscous fluid allows the formation of lubricated threads that are susceptible to a variety of hydrodynamic instabilities. These nearly cylindrical fluid threads result from the tendency of the system to minimize viscous dissipation for large viscosity contrasts, $\chi \gg 1$ [21].

In this section, we study the miscible fluid thread formed by the dispersed phase at the hydrodynamic flow focusing section, for a viscosity ratio of $\chi = 20$. Before entering the Hele-Shaw cell, the thread undergoes an instability that causes it to oscillate, due to small perturbations inside the main microchannel. Inside the chamber, the thread's velocity decreases as it passes through the widening section and displays folding patterns at the entrance of the chamber, as shown in Fig. 3. This deceleration causes the thread to expand and occupy a large portion of the microfluidic chamber.

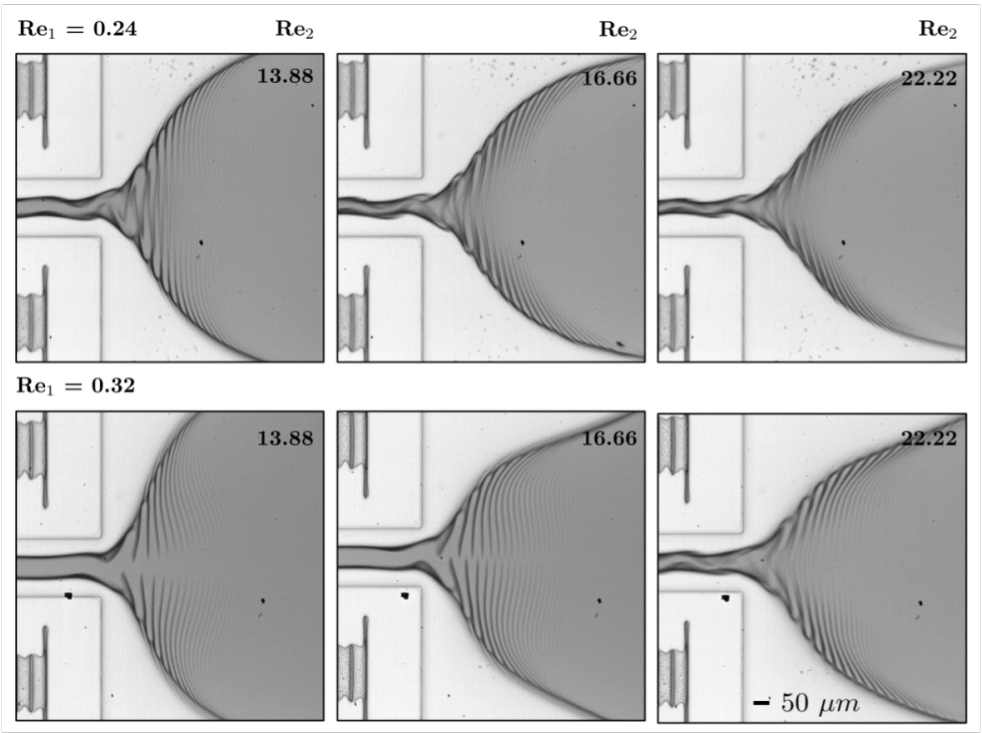

Fig. 3 – Series of details showing folding patterns in the Hele-Shaw cell for a fluid pair with $\chi = 20$.

The flow patterns presented above develop for a relatively low Reynolds number for the dispersed phase $\mathrm{Re}_1 < 1$ and for higher Reynolds numbers for the continuous

phase $\mathrm{Re}_2 > 10$. For both phases, the Reynolds number is calculated using:

$$\mathrm{Re}_i = \frac{\rho_i V_i D_h}{\eta_i} \rightarrow \mathrm{Re}_i = \frac{4\rho_i Q_i}{\eta_i P}, \tag{1}$$

where ρ is the density of the fluid, $V = Q/A$ is the velocity of the fluid phase, with Q being the inlet flow rate and A the area of the square inlet microchannel ($w = h = 100$ µm), $D_h = 4A/P$ is the hydraulic diameter, with P being the perimeter of the inlet microchannel, η is the viscosity, and index $i = 1$ or 2 refers to the fluids 1 - the dispersed phase or 2 - the continuous phase.

A parameter suitable for describing the flow of miscible liquid pairs is the Péclet number, representing the ratio between advection and diffusion. The Péclet number ranges between 10^4 and $4 \cdot 10^4$ in the main microchannel, and therefore the miscible fluid thread flow mainly through advection. The velocity of the dispersed phase V_1 typically ranges between 10^{-2} and 10^{-1} m/s and that of the continuous phase V_2 between 10^{-1} and $3 \cdot 10^{-1}$ m/s. The diffusion coefficient of the water-glycerol system is 930 µm^2/s [22]. The Péclet number was calculated using [8]:

$$\mathrm{Pe} = \frac{h(V_1 + V_2)}{\mathcal{D}}, \tag{2}$$

where h is the height of the microchannel, V_1 and V_2 are the velocities of the fluids and $\mathcal{D}$ is the diffusion coefficient.

The velocities V_1 and V_2 are determined by expressing them as:

$$V_i = \frac{Q_i}{h^2}. \tag{3}$$

We first examine the influence of the inlet flow rates of the fluid phases on the diameter ε of the viscous thread. We measure ε in the main microchannel and show that, for flow rate ratios $\varphi < 0.4$, the thread diameter in dimensionless form $\varepsilon^* = \varepsilon/h$, where h is the height of the microchannel, increases linearly with the flow rate ratio, as shown in Fig. 4. In other words, if the flow rate of the dispersed phase is increased, while keeping the other flow rate fixed, the viscous fluid thread also increases in diameter. For flow rate ratios $\varphi > 0.4$, yielding that Q_1 is almost half of Q_2, the thread diameter reaches a constant value of approximately $\varepsilon^* = 0.92$. This fact is due to the confinement provided by the main microchannel's walls before the entrance in the Hele-Shaw cell.

The viscous threads exhibit periodic oscillations before entering the microfluidic chamber depending upon the inlet flow rates. Figure 5 shows the measured oscillation frequency of the fluid thread as a function of the flow rate ratio, having kept the inlet flow rate of the dispersed phase Q_1 constant. We observe that the oscillation frequency of the fluid thread decreases, as the flow rate ratio is increased. This is due to the inertia induced by the tendency of the fluid thread to increase in diameter with the flow rate ratio.

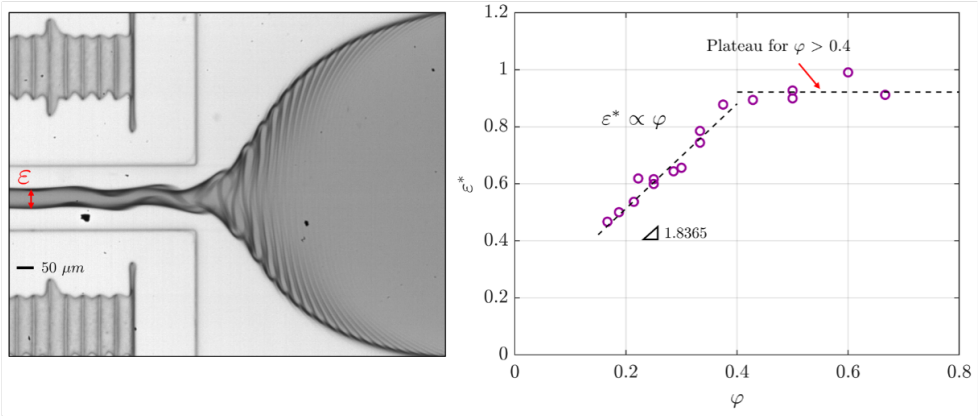

Fig. 4 – The fluid thread's diameter in dimensionless form as a function of the flow rate ratio.

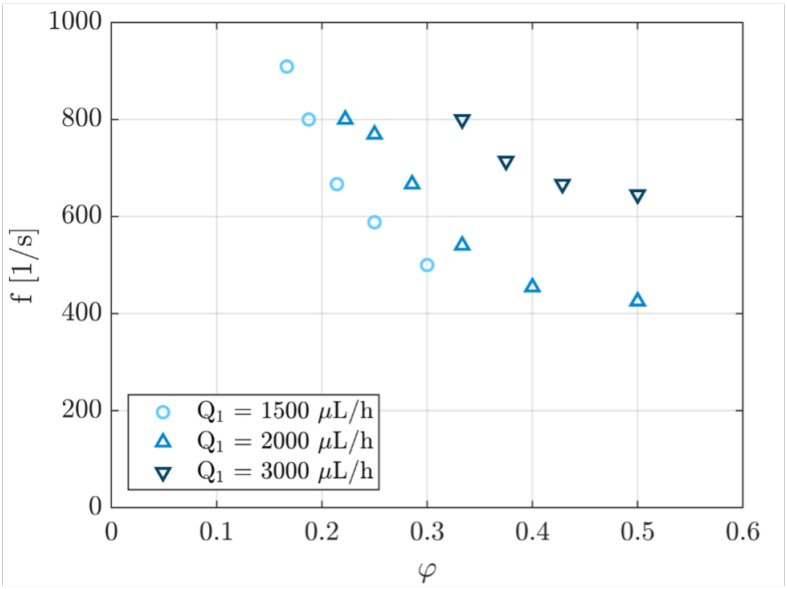

Fig. 5 – Oscillation frequency of the viscous fluid thread as a function of the flow rate ratio.

We propose a dimensionless representation in terms of a modified Strouhal number as a function of the flow rate ratio. The Strouhal number for the dispersed phase is given by:

$$\mathrm{Sh}_1 = \frac{fL}{V_1} \rightarrow \mathrm{Sh}_1 = \frac{f\pi\varepsilon^3}{4Q_1}, \tag{4}$$

where f is the oscillation frequency of the viscous thread, L is the characteristic dimension, and in this case $L = \varepsilon$, where ε is the measured thread diameter, $V_1 = Q_1/(\pi\varepsilon^2/4)$ is the velocity of the dispersed phase, with Q_1 being the inlet flow rate of the dispersed phase.

As shown in Fig. 6, the data follow a power law of the form $\mathrm{Sh}_1 \approx 0.89\varphi^{0.91}$, which could be used to approximate the oscillation frequency of the viscous thread at any given flow rate ratio φ. One can observe from the dimensionless representation that the Strouhal number Sh_1 increases with the flow rate ratio, emphasizing a stronger dependency on the thread's diameter.

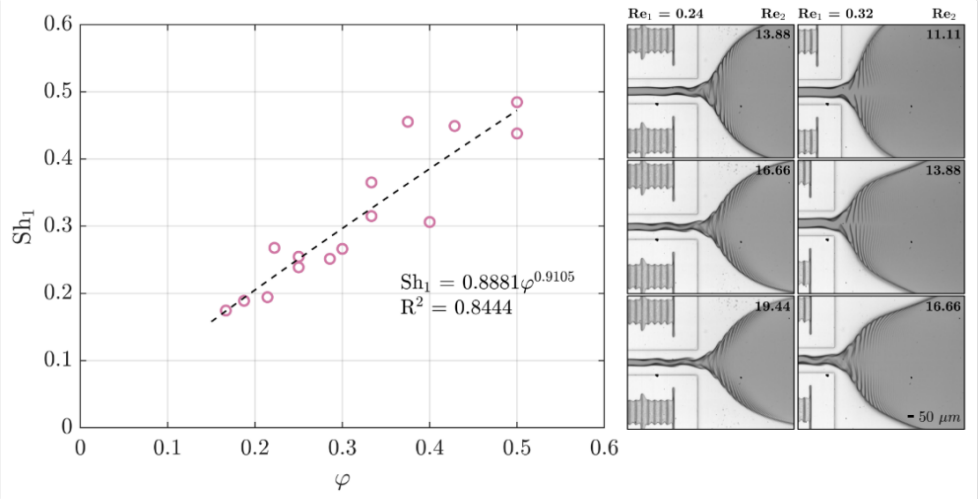

Fig. 6 – Strouhal number for the dispersed phase as a function of flow rate ratio.

3.2. FLOW REGIMES DISPLAYING THE KELVIN-HELMHOLTZ INSTABILITY

By increasing the viscosity contrast between the two injected miscible fluids at $\chi = 55$, we report for the first time the development of the Kelvin-Helmholtz instability in a Hele-Shaw cell (see Fig. 7). This instability arises when there is a velocity contrast at the apparent interface between two miscible fluids [23] and it is characterized by the formation of vortices across the interface. The Péclet numbers are Pe$> 10^4$, hence the diffusion effects are negligible, and the advection is the main process by which momentum is transferred.

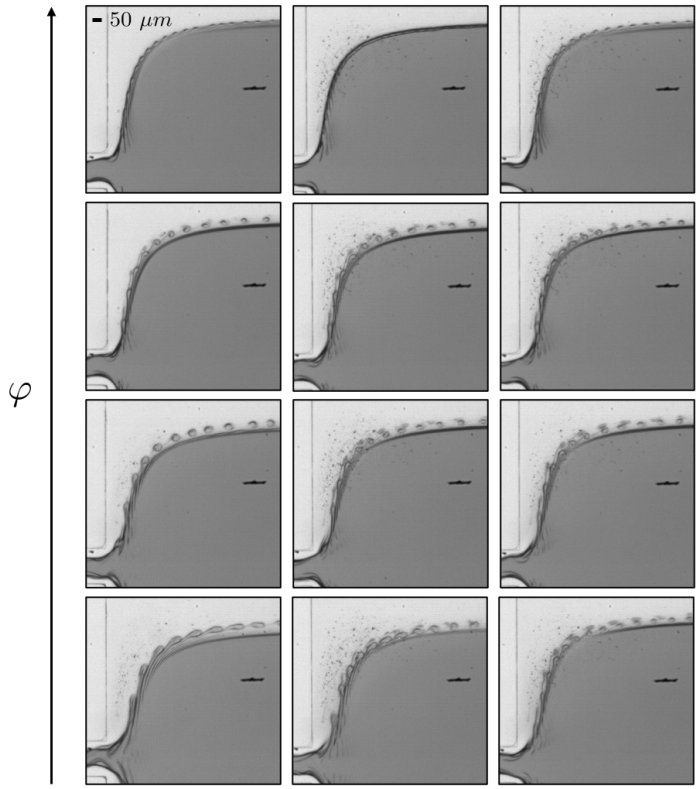

Fig. 7 – Depiction of the Kelvin-Helmholtz instability in the Hele-Shaw cell for a fluid pair with a viscosity contrast of 55.

Right after the cross section, we note that the viscous fluid thread starts to oscillate periodically. We measure the oscillation frequency f by keeping the flow rate of the dispersed phase Q_1 constant and represent it as a function of the flow rate ratio φ in Fig. 8a. In all five cases, the oscillation frequency decreases as the flow rate ratio is increased. We propose a dimensionless representation of the oscillation frequency by calculating the Strouhal number corresponding to the dispersed phase Sh_1 using relation (4) and show that the experimental data follow a power law when representing them as a function of the flow rate ratio, as seen in Fig. 8b.

The vortices form right at the entrance of the Hele-Shaw cell, when the fluid thread starts to widen. As they advance at the apparent interface between the two phases, they separate. This results in an approximately equal distance between the vortices, and they remain intact until they reach the outlet microchannel of the chamber. To gain insight into the dynamics of the vortices, we measure their radius and represent $R^* = R/\varepsilon$ as a function of the flow rate ratio φ in Fig. 9. We observe that the radius

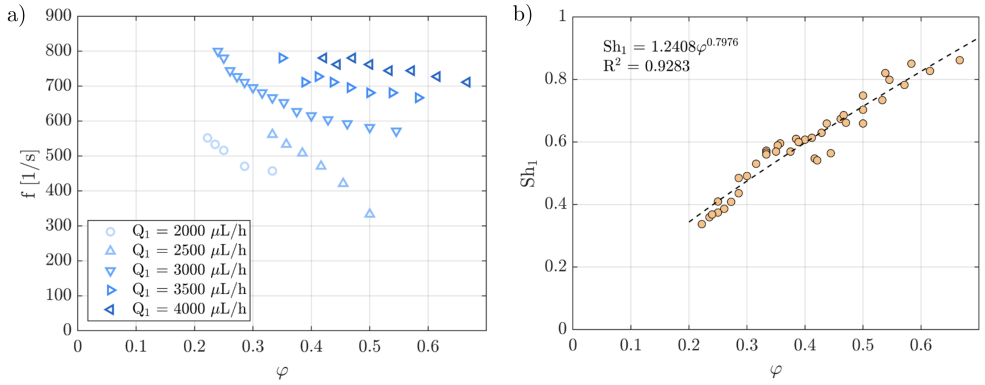

Fig. 8 – Oscillation frequency of the viscous fluid thread (a) and Strouhal number (b) for the dispersed phase as functions of the flow rate ratio.

of the vortices decreases with the flow rate ratio, following a power law. If the flow rate of the dispersed phase is increased, the vortices have less time to accumulate at the entrance of the microfluidic chamber and therefore, they tend to shed more frequently, and their radius decreases.

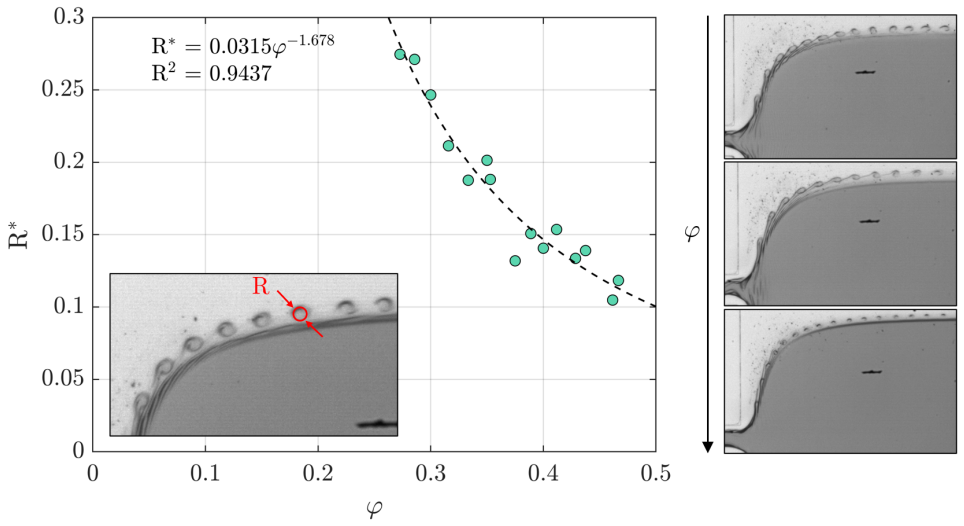

Fig. 9 – Radius of the vortices in dimensionless form as a function of the flow rate ratio.

3.3. FOLDING INSTABILITIES OF VISCOUS FLUID THREADS

Experiments are carried out in the Hele-Shaw cell to probe and manipulate viscous buckling instabilities, by increasing the viscosity ratio of the miscible fluid

pair at $\chi = 100$. We observe that the fluid filament is highly stable from the formation region (at the cross section) until the entrance of the microfluidic chamber. The dispersed phase has a higher viscosity than the water-glycerol solutions we investigated in the previous sections, which leads to the stabilization of the filament in the main microchannel, making it less susceptible to instabilities in that region of the microfluidic device. When the fluid filament enters the Hele-Shaw cell, an axial compressive stress is generated along the decelerating fluid thread that causes it to bend and fold [24]. As the viscous thread advances, its dilation due to the geometry prohibits significant folding.

The Reynolds numbers for the investigated folding regime are $\mathrm{Re}_1 \approx 10^{-3}$, while Re_2 varies between 1 and 10. We investigate the behavior of the miscible fluid threads in a flow regime where diffusion effects are negligible, provided that the Péclet number is high $\mathrm{Pe} \approx 10^3$ - 10^4.

We first focus on measuring the diameter of the fluid filament ε in the main microchannel, away from the hydrodynamic instability generated in the Hele-Shaw cell. We find that, in dimensionless form ε^*, the diameter of the viscous thread increases linearly with the flow rate ratio φ, as shown in Fig. 10.

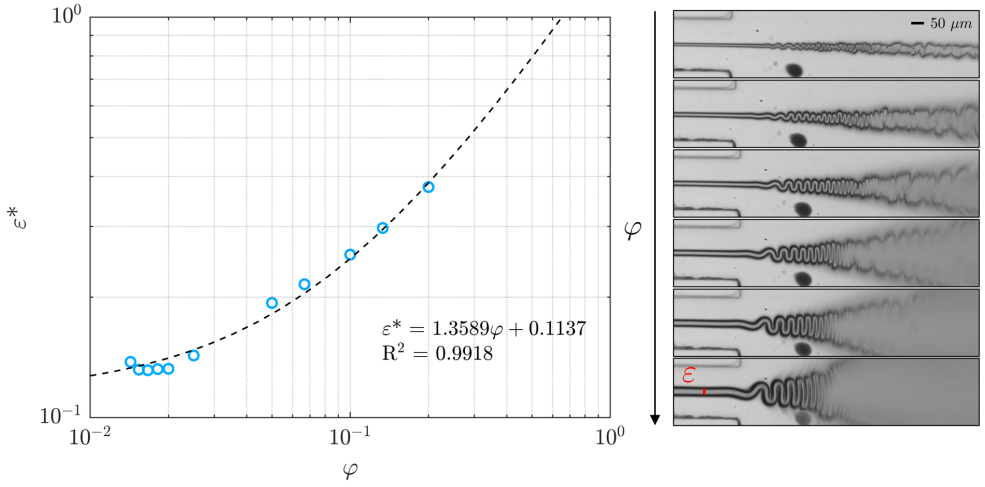

Fig. 10 – Diameter of the viscous fluid thread in dimensionless form as a function of the flow rate ratio.

As mentioned earlier, the system exhibits a periodic behavior, where the viscous fluid thread folds in the microfluidic chamber, due to a sudden change in the thread's velocity as it passes through the widening section of the device. We measure this folding frequency and show that it can be reduced by increasing the flow rate ratio, as depicted in Fig. 11a. This observation is also suggested by the representation of a modified Strouhal number calculated for the dispersed phase Sh_1, where the

characteristic dimension is considered the width of the main microchannel, as a function of the flow rate ratio φ (see Fig. 11b). The data follow a power law that could generally be used to predict the oscillation frequency of the viscous fluid thread at any given flow rate ratio. The Strouhal number is calculated using the following expression:

$$\mathrm{Sh}_1 = \frac{f D \pi \varepsilon^2}{4 Q_1}, \tag{5}$$

where f is the oscillation frequency, D is the width of the main microchannel, ε is the diameter of the fluid filament and Q_1 is the inlet flow rate of the dispersed phase.

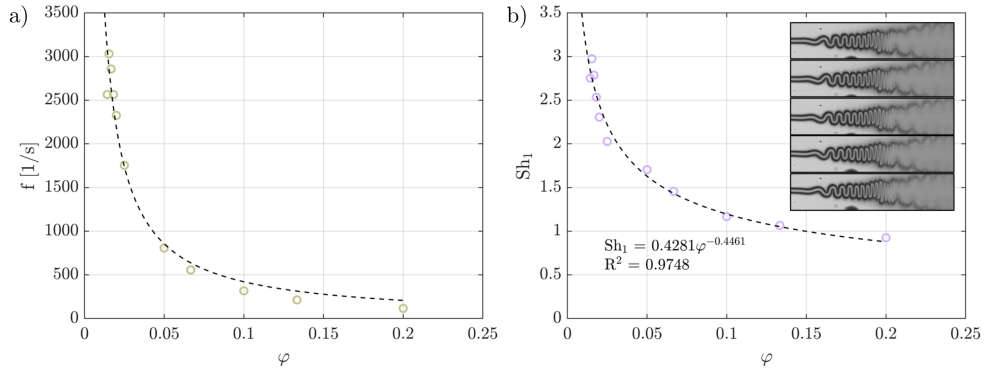

Fig. 11 – Oscillation frequency of the viscous fluid thread (a) and Strouhal number (b) calculated for the dispersed phase as functions of the flow rate ratio.

4. CONCLUSIONS

In this paper, we provide a detailed examination of hydrodynamic instabilities at the microscale by varying the viscosity contrast of three miscible fluid pairs. The first investigated instability, for a viscosity contrast of the liquid pair of 20, consists of the oscillation of viscous fluid threads and the onset of folding morphologies as the threads enter the Hele-Shaw cell. We find that diameter of the viscous thread increases with the flow rate ratio, provided that $\varphi < 0.4$. Conversely, for flow rate ratios greater than 0.4, the thread diameter reaches a plateau of $\varepsilon^* = 0.92$, as a result of wall confinement. Moreover, we show that the oscillation frequency of the fluid thread decreases with the flow rate ratio due to the inertia of the fluid threads. A dimensionless representation of the Strouhal number for the dispersed phase as a function of the flow rate ratio reveals that our data can be approximated by a power law.

A Kelvin-Helmholtz instability is reported for the first time in a Hele-Shaw cell where diffusion effects are negligible, by increasing the viscosity contrast of the

miscible fluid pair at 55. We find that the oscillation frequency of the viscous fluid thread decreases with the flow rate ratio, while the Strouhal number for the dispersed phase increases with the flow rate ratio, following a power law. In addition to these results, we experimentally observe the formation of vortices across the apparent interface between the fluids in the microfluidic chamber. We measure the radius of the vortices and represent them in dimensionless form as a function of the flow rate ratio. We conclude that, as the flow rate of the dispersed phase is increased, the vortices can no longer accumulate at the breaking point and their radius decreases.

We report another hydrodynamic instability by increasing the viscosity contrast to 100, which is the bending and folding of viscous fluid threads in the Hele-Shaw cell. The viscous thread is highly stable until it enters the microfluidic chamber, due to the higher viscosity of the dispersed phase. We measure and find that the diameter of the fluid thread increases linearly with the flow rate ratio.

The present scientific findings provide insight into new hydrodynamic instabilities that occur at the microscale. Also, the paper represents an exploratory study in the field of microfluidics that expands the current knowledge of miscible fluid flows in Hele-Shaw cells. We show how pairs of viscous miscible fluids interact in a confined device and emphasize some predictable aspects of the investigated fluid structures. The results are relevant in fields such as biomedical, chemical or petroleum engineering due to its applicative potential for emphasizing microfluidic flows that can lead to enhanced fluid manipulation strategies at the microscale.

Acknowledgements. This work was supported by a grant of the Ministry of Research, Innovation and Digitization, CNCS-UEFISCDI, project number PN-IV-P2-2.1-TE-2023-0288, within PNCDI IV and by a grant from the National Programme for Research of the National Association of the Technical Universities (GNAC ARUT 2023). The authors would like to thank Eugen Chiriac for his support and technical insights during the manufacturing process of the Hele-Shaw cell.

REFERENCES

1. P. Guillot and A. Colin, "Stability of parallel flows in a microchannel after a T junction", Phys. Rev. E Stat. Nonlin. Soft Matter Phys. **72**, 066301 (2005).
2. G. F. Christopher, N. N. Noharuddin, J. A. Taylor, and S. L. Anna, "Experimental observations of the squeezing-to-dripping transition in T-shaped microfluidic junctions", Phys. Rev. E Stat. Nonlin. Soft Matter Phys. **78**, 036317 (2008).
3. T. Cubaud, M. Tatineni, X. Zhong, and C. M. Ho, "Bubble dispenser in microfluidic devices", Phys. Rev. E Stat. Nonlin. Soft Matter Phys. **72**, 037302 (2005).
4. T. Cubaud and T. G. Mason, "Capillary threads and viscous droplets in square microchannels", Phys. Fluids **20**, 052103 (2008).
5. S. Darvishi and T. Cubaud, "Lubrication of highly viscous core-annular flows in microfluidic chambers", J. Fluids Eng. **133**, 031101 (2011).
6. T. Cubaud, "Segmented flows of viscous threads in microchannels", Phys. Rev. Fluids **4**, 084201 (2019).

7. S. Darvishi and T. Cubaud, "Viscous core-annular flows in microfluidic chambers", ASME 2010 8th Int. Conf. Nanochannels, Microchannels, Minichannels (parts A and B), 1593–1600 (2011).
8. T. Cubaud and S. Notaro, "Regimes of miscible fluid thread formation in microfluidic focusing sections", Phys. Fluids **26**, 122005 (2014).
9. M. Hashimoto, P. Garstecki, H. A. Stone, and G. M. Whitesides, "Interfacial instabilities in a microfluidic Hele-Shaw cell", Soft Matter **4**, 1403–1413 (2008).
10. T. Dinh, Y. Xu, T. G. Mason, and T. Cubaud, "Microflow of nanoemulsion threads in surfactant solutions", Phys. Rev. E **107**, 015101 (2023).
11. H. Wang, B. Wei, J. Hou, Z. Sun, Q. Du, and K. Zhou, "Investigation of microflow mechanisms and emulsion size distribution in porous media", Phys. Fluids **35**, 102003 (2023).
12. S. M. Yang, S. Lv, W. Zhang, and Y. Cui, "Microfluidic point-of-care (POC) devices in early diagnosis: A review of opportunities and challenges", Sensors **22**, 1620 (2022).
13. W. Su, X. Gao, L. Jiang, and J. Qin, "Microfluidic platform towards point-of-care diagnostics in infectious diseases", J. Chromatogr. A **1377**, 13–26 (2015).
14. C. D. Chin *et al.* "Microfluidics-based diagnostics of infectious diseases in the developing world", Nat. Med. **17**, 1015–1019 (2011).
15. L. Kong *et al.* "Lipid-stabilized double emulsions generated in planar microfluidic devices", Langmuir **36**, 2349–2356 (2020).
16. W. Wang *et al.* "Microfluidic emulsification techniques for controllable emulsion production and functional microparticle synthesis", Chem. Eng. J. **452**, 139277 (2023).
17. Y. Liu, L. Sun, H. Zhang, L. Shang, and Y. Zhao, "Microfluidics for drug development: From synthesis to evaluation", Chem. Rev. **121**, 7468–7529 (2021).
18. I. Maimouni, C. M. Cejas, J. Cossy, P. Tabeling, and M. Russo, "Microfluidics mediated production of foams for biomedical applications", Micromachines **11**, 83 (2020).
19. M. Hashimoto, P. Garstecki, and G. M. Whitesides, "Synthesis of composite emulsions and complex foams with the use of microfluidic flow-focusing devices", Small **3**, 1792–1802 (2007).
20. W. Wang, M. J. Zhang, and L. Y. Chu, "Microfluidic approach for encapsulation *via* double emulsions", Curr. Opin. Pharmacol. **18**, 35–41 (2014).
21. T. Cubaud and T. G. Mason, "Folding of viscous threads in diverging microchannels", Phys. Rev. Lett. **96**, 114501 (2006).
22. W. Hayduk and H. Laudie, "Prediction of diffusion coefficients for nonelectrolytes in dilute aqueous solutions", AIChE J. **20**, 611–615 (1974).
23. C. Liu, H. Xu, X. Cai, and Y. Gao, *Liutex and Its Applications in Turbulence Research*, Springer, Singapore, 1–230, 2020.
24. T. Cubaud, B. M. Jose, and S. Darvishi, "Folded micro-threads: Role of viscosity and interfacial tension", Phys. Fluids **23**, 042101 (2011).